Optimization of Continuous One-Dimensional Structures under Steady Harmonic Excitation

Erwin H. Johnson*
NASA Ames Research Center, Moffett Field, Calif.
Paulo Rizzi,† Holt Ashley‡
Stanford University, Stanford, Calif.
and
Solly A. Segenreich§
COPPE-Federal University of Rio de Janeiro, Rio de Janeiro, Brazil

To illustrate the minimum-weight design of one-dimensional, elastic structures under dynamic excitation, methods from optimal control theory are applied to the cantilever bar driven sinusoidally by an axial force at its tip. Other directly analogous problems are identified, and closely related cases are discussed along with practical applications. Realistic constraints are enforced during the optimizations: maximum allowable stress amplitude at any point along the bar and the minimum cross-sectional area. In the absence of damping, the design space may contain many disjoint feasible regions, and multiple optima can exist. This novel feature is examined, first by reference to a simple example with only two element areas to determine. Solutions are worked out in detail for continuous bars, with the excitation frequency less than, then greater than, the fundamental free-vibration frequency. The latter results overcome a limitation inherent in previous analyses. Above a certain excitation frequency, two or more arcs with different constraints characterize the optimal designs; a concentrated tip mass is also needed in some cases. Free vibrations of the optimal designs are analyzed. Background on the difficulties of going to even higher frequencies than those covered by the exact solutions is covered by a discussion of forced-response mode shapes, by reference to finite element results, and by a simplified two-design-variable example.

I. Introduction and Summary of Previous Research

THIS paper examines some questions relating to the optimal design of continuous, one-dimensional structures driven by harmonically oscillating loads. The subject matter differs in two respects from most research being done in the rapidly expanding field of structural optimization: (a) the examples studied are subjected to dynamic excitation, without limits on the frequency of the loading, and (b) the emphasis is on continuous structural representation, so that differential equations rather than finite elements are used in searching for the optimum.

The time-dependent forcing produces distributed inertial loads, which can have important effects on the solutions. Furthermore, the possible resonances associated with sinusoidal motion give rise to disconnected feasible regions in the design space and to numerous local optima – phenomena that have rarely received systematic attention in the past.

The use of differential equations naturally draws on the calculus of variations as it has been extensively developed in the field of optimal control theory (see Ref. 1, Chapts. 2 and 3). These methods are applied here to illustrate some interesting features that harmonic excitation introduces into minimum weight design. The cases chosen are merely typical, in that many other one-dimensional structures can be synthesized in an analogous fashion.

With regard to related previous work, structural optimization has been an active field for nearly two decades. A survey paper focused on continuous representations was published by Sheu and Prager[2] in 1968 and provides an excellent review up to that date. Two more recent symposium proceedings, edited by Gellatly[3] and Schmit,[4] provide "state-of-the-art" descriptions of the field. These three reports emphasized static loadings, whereas a survey paper by Pierson[5] reviewed structural optimization in free and forced dynamic environments; conditions that correspond to the topic of this paper. As of 1972, Pierson states his conclusions that the field is "still in its infancy" and that "there is a notable lack of published work" in the forced dynamic response category. A more recent review of this topic by Rao[6] confirms that these conclusions are still valid today.

The series of investigations most directly antecedent to the present one are those of Icerman,[7] Mroz,[8] and Plaut.[9] All employ energy methods connected with Rayleigh's inequality to design minimum-weight structures under simple harmonic excitation. A common feature of their approaches is that the forcing frequency is limited from above by the fundamental natural frequency of the optimal configuration. Two contributions of the present study are the removal of this limitation and the imposition of conditions deemed more realistic than those of Refs. 7-9 (see Sec. II). In addition, the authors are not aware of previous results, in the structures area, which successfully treated state variable inequality constraints with analytic methods.

Finally it should be recognized that most of the material in the following section derives from portions of doctoral theses

Presented at the AIAA/ASME/SAE 17th Structures, Structural Dynamics and Materials Conference, King of Prussia, Pa., May 5-7, 1976 (in bound volume of Conference papers, no paper number); submitted May 7, 1976; revision received Sept. 23, 1976. This research was supported in part by the Air Force Office of Scientific Research (contract AFOSR 74-2712) and in part by NASA Grant NGL-05-020-243. The authors are indebted to John V. Breakwell, Stanford University, for valuable discussions of the mathematics of optimization, as well as to Arthur E. Bryson, Jr., for suggesting the two-design-variable example of Sec. VI.

Index categories: Structural Design, Optimal; Structural Dynamic Analysis.

*NRC Postdoctoral Research Associate; presently Engineering Specialist, Northrop Corp., Aircraft Division. Associate Member AIAA.

†Graduate Student, Dept. Aeronautics and Astronautics.

‡Professor, Dept. Aeronautics and Astronautics. Fellow AIAA.

§Assistant Professor. Member AIAA.

by two of the authors (Johnson[10] and Rizzi[11]). Reference 10, in particular, uses finite element structural representation and computer searches based on mathematical programming to find a variety of optimal one-dimensional structures subjected to harmonic or random forcing. Both theses contain numerous references to related works that could not be mentioned here due to space limitations. Most of these additional references treat structural optimization either with free vibration and aeroelastic constraints or with transient, as opposed to harmonic, loading conditions.

II. Statement of Focal Problem and Its Analogs

To introduce somewhat more realistic design criteria than used in related previous investigations, the following example is selected for study here: the cantilever bar in Fig. 1a undergoes steady harmonic response to an oscillating axial load at its tip. A limit is imposed on the maximum amplitude of oscillatory stress $\sigma(x)e^{i\omega_e t}$, and a "minimum-gauge" constraint is placed on the cross-sectional area $A(x)$. The optimal area distribution is sought in the sense of minimum volume (or weight). When the effects of transient response to load startup can be neglected, this problem statement is believed closer to what a designer would encounter than, for example, the effective limitation on tip amplitude of Icerman[7] or the "minimum dynamic compliance" used by Mroz.[8]

When writing differential equations and boundary conditions for a continuum model of the bar, allowance is made for a concentrated mass $M_T \geq 0$ at the tip. Under some circumstances, M_T is required as part of the optimal solution, but in vibration-isolation applications it might also represent that portion of the isolated mass supported by the particular mount being designed. In terms of the format favored in optimal-control theory, the problem can be written in dimensionless terms:

minimize a quantity proportional total bar weight,

$$J = a_T + \int_0^1 a(s)\,ds, \tag{1}$$

subject to a stress constraint,

$$|\sigma/E| \leq \beta \equiv \sigma_{\max}/E \tag{2}$$

a minimum area constraint,

$$a(s) \geq 1/\delta \equiv A_{\min}\sigma_{\max}/P \tag{3}$$

and the steady-state differential equation

$$(d/ds)[a(s)\,(dv/ds)] + 2\alpha^2 a(s)v(s) = 0 \tag{4}$$

with the boundary conditions

$$v(0) = 0 \qquad a(1)[dv(1)/ds] = \beta + 2\alpha^2 a_T v(1) \tag{5}$$

In terms of the dimensional parameters u, E, ρ, $\sigma_{\max}$, and P (which are, respectively, the axial displacement, Young's modulus, structural density, the maximum allowable stress and the applied tip load) the dimensionless quantities in Eqs. (1)-(5) are defined as follows

$$s = x/\ell$$

$$v(s) = u/\ell$$

$$a(s) = A\,\sigma_{\max}/P$$

$$a_T = M_T\,\sigma_{\max}/\rho\ell P$$

$$\alpha^2 = (\omega_e \ell)^2 \rho/2E \tag{6}$$

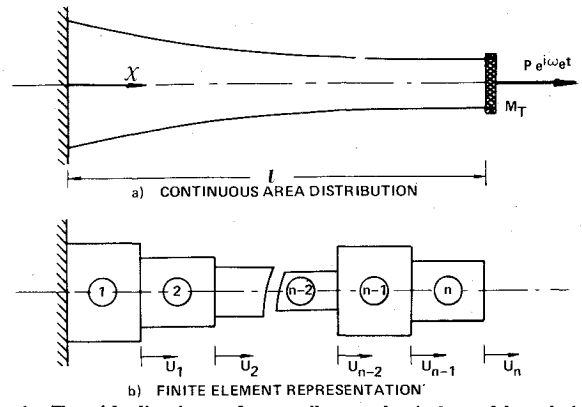

Fig. 1 Two idealizations of a cantilever, elastic bar of length ℓ, excited in axial vibration by a sinusoidally varying force at the free end. A concentrated mass M_T may be attached at the tip. For finite-element modeling, the bar is divided into n uniform segments of equal length.

Note that the dimensionless area parameter δ of Eq. (3) couples the minimum allowable area, $A_{\min}$, with the stress limitation and the amplitude of the applied tip force. Furthermore, perhaps it should be stressed that the nondimensional tip mass, a_T, appears in the "cost function" of Eq. (1) as a discrete control variable.

In preparation for an attack by the methods of optimal control theory, one must express Eq. (4) in the "state vector" form of a pair of first-order equations. The definitions

$$x_1 \equiv v \tag{7}$$

$$x_2 \equiv a(dv/ds) \tag{8}$$

thus leads to

$$\dot{x}_1 = x_2/a \tag{9}$$

$$\dot{x}_2 = -2\alpha^2 a x_1 \tag{10}$$

The boundary conditions and constraints are

$$x_1(0) = 0 \tag{11}$$

$$x_2(1) - \beta - 2\alpha^2 a_T x_1(1) = 0 \tag{12}$$

$$|x_2|/a - \beta \leq 0 \tag{13}$$

$$-a(s) + 1/\delta \leq 0 \tag{14}$$

Two other structural configurations occur in vibration isolation, force transmission, and related technologies, whose design for minimum weight is mathematically analogous to the bar. These are the thin-walled cantilever rod undergoing torsional excitation at its free tip and a stubby cantilever beam whose lateral displacements are governed by its shear rigidity (see Ref. 12).

III. The Question of Multiple Feasible Regions

In his comprehensive illuminating study of minimum-weight frames subjected to transient dynamic excitation, Cassis[13] concludes: "It was found that the design space may have disjoint feasible regions that are due to the sinusoidal contributions to the dependence of the dynamic response functions on the design variables. This fundamental and important characteristic had not been anticipated, nor was it previously recognized in the structural optimization literature." The authors believe the class of problems treated here to be unique in its involvement with such multiple, disjoint feasible regions. In fact, there appear to be

denumerable infinity of regions, each associated with an excitation frequency ω_e that falls in the range $\omega_i < \omega_e < \omega_{i+1}$, where ω_i is the ith free-vibration frequency of the corresponding optimal bar, rod, etc. The design space of the continuous bar is an "infinite-dimensional" function space, and it is somehow characterized by insurmountable "barriers" between feasible regions, along which resonant response occurs near each $\omega_e = \omega_i$.

Earlier solutions have avoided this difficulty because their requirement that $\omega_e < \omega_1$ eliminates the ambiguity. Although optimality criteria like those of Icerman[7] and Mroz[8] do seem to be both necessary and sufficient for the "absolute minimum" designs thus produced, this is accomplished at the price of ruling out other possible superior designs that meet all the stated conditions other than $\omega_e < \omega_1$. The methods of variational calculus adopted here are admittedly weaker in that it is harder to examine the sufficiency or "globality" of the solutions obtained from the necessary conditions they furnish. Yet they yield satisfactory, practical designs that are clearly local optima and that tempt an engineer to postpone the detailed examination of sufficiency.

Johnson[10] studied a case, with just two design variables, that illustrates the situation simply and graphically. Slightly modified to conform with the problem in Sec. II, it consists of a bar with two equal-length segments of areas a_1 (near the cantilever root) and a_2 (near the tip). It is driven at the tip by force $Pe^{i\omega_e t}$; a_1 and a_2 are to be selected for minimum weight, with specified minimum gauges and constraints on maximum allowable stress amplitude. Starting from differential equations of the uniform bar in each segment, the problem can be solved exactly. The straightforward mathematical details are omitted here.

Figures 2a and b depict design spaces for the two-segment bar at two values of the forcing-frequency parameter α from Eq. (6). Feasible portions of these spaces are left unshaded; total weight (proportional to $a_1 + a_2$) is constant along the 45° sloping lines used to shade the infeasible regions. The required minimum areas are $a_1 = a_2 = 0.2$. Evidently, a 50% increase in α has moved the "global optimum" from the vertex of the right-hand region to that of the second region in the upper left-hand corner. Furthermore, the proportions of the minimum-weight bar have changed radically, from one having nearly uniform cross section to one with a thick tip section and a minimum-gauge root.

The explanation of this behavior is to be found by studying the dimensionless vibration eigenvalues $\alpha_i = \omega_i \ell \sqrt{\rho/2E}$, $i = 1, 2$, of the system. In Fig. 2a, the designs with the fundamental α_1 equal to $\alpha = 0.707$ can all be shown to lie on the dashed straight line

$$a_1 = 0.198\ a_2 \tag{15}$$

It proceeds through the middle of the infeasible region and constitutes the "maximum of infeasibility," because along it the resonant response is unbounded. Below this line, $\alpha_1 > \alpha$ and conversely; each of the associated feasible regions clearly offers its own optimum.

By an extension of the work of Segenreich and Rizzi,[14] it can be proved that segmented cantilevers modeled in this fashion have bounds on their eigenvalues. In the present case of two equal segments, these limits are

$$\frac{(i-1)\pi}{\sqrt{2}} \leq \alpha_i \leq \frac{i\pi}{\sqrt{2}} \tag{16}$$

for $i = 1,2,3,\ldots$. It follows that there will be two feasible regions for each nonzero excitation frequency. (In the static case, $\alpha = 0$, the fully stressed solution is the single optimum.) Both situations graphed in Fig. 2 therefore permit two regions.

In principle, the foregoing line of reasoning can be extended to one-dimensional discrete models with an arbitrary

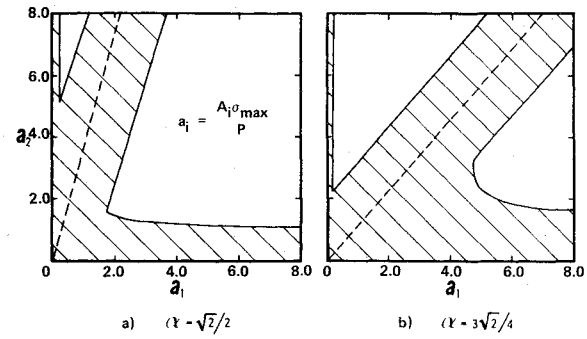

Fig. 2 Illustrating the feasible design spaces (unshaded) for a simple, two-element bar forced from its tip at the two indicated values of dimensionless frequency α; a_1 and a_2 are dimensionless areas adjacent to the root and tip, respectively.

number of segments. It also motivates the hypothesis of a denumerable infinity of local optima for continuous structures. More details are given in Ref. 14 and in a recent paper by Johnson.[15]

It might be supposed that the disjoint design space results from the omission of any structural damping, and this is strictly true. When damping is provided, the infinitely high "ridges" disappear and the infeasible regions no longer extend to infinity. However, even with unrealistically high amounts of structural energy dissipation, it is found[10] that many "pockets of feasibility" remain in the unified design space. The basic problem of singling out a global optimum from several local candidates persists.

IV. Optimization of the Continuous Bar

As set forth, for instance, in Secs. 2.4, 3.8, and 3.12 of Ref. 1, necessary conditions for a minimum of J in Eq. (1) under the constraints and boundary conditions (7)-(14) may be constructed from the Hamiltonian

$$H = a + \lambda_1 \frac{x_2}{a} - \lambda_2 2\alpha^2 a x_1 + \mu_1\left(\frac{|x_2|}{a} - \beta\right) + \mu_2\left(\frac{1}{\delta} - a\right) \tag{17}$$

Here $\lambda_i(s)$, $\mu_i(s)$ are Lagrange multipliers that introduce the respective constraints factored by them and $a(s)$ is the "control variable."

By setting the variations of J with respect to a, the state variables x_1, x_2, and possibly a_T equal to zero, the "control equation" and the equations for the adjoint variables are obtained

$$1 - \lambda_1 \frac{x_2}{a^2} - \lambda_2 2\alpha^2 x_1 - \mu_1 \frac{|x_2|}{a^2} - \mu_2 = 0 \tag{18}$$

$$\dot{\lambda}_1 = 2\alpha^2 a \lambda_2 \tag{19}$$

$$\dot{\lambda}_2 = -\frac{\lambda_1}{a} - \mu_1 \frac{\operatorname{sgn}(x_2)}{a} \tag{20}$$

If a_T (i.e., M_T) is not prescribed to be a constant or zero, a special boundary condition

$$1 - \nu_1 2\alpha^2 x_1(1) - \nu_2 = 0 \tag{21}$$

arises, where ν_1 and ν_2 are constants, to be determined. From integrations by parts in the variational process, the following additional boundary conditions are found

$$\lambda_2(0) = 0 \tag{22}$$

$$\lambda_1(1) = -\nu_1 2\alpha^2 a_T \tag{23}$$

$$\lambda_2(1) = \nu_1 \tag{24}$$

Finally, the nonnegativity conditions on the multipliers are

$$\mu_1 = \begin{cases} 0\ , & \text{if } |x_2|/a < \beta \\ \geq 0, & \text{if } |x_2|/a = \beta \end{cases} \tag{25}$$

$$\mu_2 = \begin{cases} 0\ , & \text{if } 1/\delta < a \\ \geq 0, & \text{if } 1/\delta = a \end{cases} \tag{26}$$

$$\nu_2 = \begin{cases} 0\ , & \text{if } a_T > 0 \\ \geq 0, & \text{if } a_T = 0 \end{cases} \tag{27}$$

Equations (21) and (27) should be disregarded when a_T is not part of the optimization.

First-Mode Solutions ($\alpha < \alpha_1$)

When the forcing frequency is less than the fundamental frequency of the optimal design, it is easily seen that the entire bar must respond in phase with the applied load

$$x_1 \geq 0, \qquad 0 \leq s \leq 1 \tag{28}$$

The tip mass will at first be omitted, as will the minimum-gauge constraint (14), for reasons that will become apparent later. It is hypothesized that the optimal design is "fully stressed" over a region or arc near the tip, with the stress constraint relaxed inboard, i.e.,

$$\frac{x_2}{a} \begin{cases} < \beta\ , 0 \leq s \leq \gamma \\ = \beta\ , \quad \gamma \leq s \leq 1 \end{cases} \tag{29}$$

where γ is a temporarily unknown matching point.

The solution is now obtained by solving Eqs. (7)-(14) and (18)-(25) separately in each of the arcs and then applying continuity conditions to find γ and the constants from the integrations. The complete details of this rather difficult solution are given by Rizzi.[11] For given values of α and β, the solution for γ is found by numerically solving the transcendental equation

$$2 - \alpha\sqrt{\pi}\exp[(\alpha/\beta)x_1(\gamma)]^2\psi\{\operatorname{erf}(\alpha\psi) - \operatorname{erf}[(\alpha/\beta)x_1(\gamma)]\} - \exp -\alpha^2\{\psi^2 - [x_1^2(\gamma)/\beta^2]\} - 2\alpha C_2\left(2\frac{x_1(\gamma)}{\beta} - \psi\right) = 0 \tag{30}$$

where erf is the error function and

$$C_2 = -\frac{\sinh(\sqrt{2}\alpha\gamma)\ \cosh(\sqrt{2}\alpha\gamma)}{\sqrt{2}} \tag{31}$$

$$x_1(\gamma) = \beta\ \tanh(\sqrt{2}\alpha\gamma)/\sqrt{2}\alpha \tag{32}$$

and

$$\psi = 1 - \gamma + \frac{x_1(\gamma)}{\beta} \tag{33}$$

When $\alpha \leq 1.0908$, this calculation shows that there is no junction point within length $0 \leq \gamma \leq 1$ of the bar. For larger α, the single meaningful root thus obtained is plotted in Fig. 3. It starts from $\gamma = 0$ with infinite slope $d\gamma/d\alpha$ and tends asymptotically to $\gamma = 1$.

Because of the manner in which P and σ_{max} enter the problem statement, a single-parameter family of solutions emerges. Five typical dimensionless area distributions $a = A\sigma_{max}/P$ are plotted in Fig. 4, for values of α increasing from the static $\alpha = 0$ to $\alpha = 1.5$ where nearly half the bar is not stress

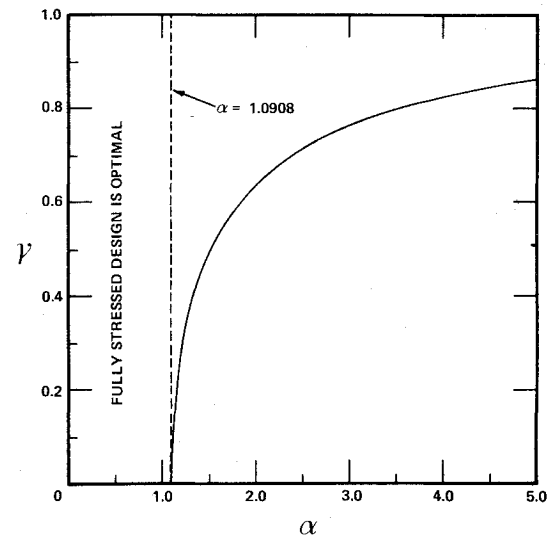

Fig. 3 Matching point $s = \gamma$ between the unconstrained and fully stressed arcs, plotted vs frequency parameter α for the first-mode designs.

constrained. Up to $\alpha = 1.0908$, however, the often-hypothesized, fully stressed design is indeed optimal. This range of excitation frequencies may often be quite wide; for instance, it applies for aluminum bars up to about $\omega_e = 3 \times 10^5/\ell$ rad/sec, where ℓ is in inches. (For shear beams and rods in torsion, the limiting frequency can be much lower.)

The area distribution of these designs may be summarized as

$$a(s) = \begin{cases} \exp\left\{\alpha^2\left[\psi^2 - \dfrac{\tanh^2(\sqrt{2}\alpha\gamma)}{2\alpha^2}\right]\right\}\left(\dfrac{\cosh\sqrt{2}\alpha\gamma}{\cosh\sqrt{2}\alpha s}\right)^2 & 0 \leq s \leq \gamma \\ \exp\{\alpha^2(1-s)[2\psi - 1 + s]\}, & \gamma \leq s \leq 1 \end{cases} \tag{34}$$

When Eq. (34) is integrated over the length, the following dimensionless weight (or volume) results

$$\frac{V\sigma_{max}}{P\ell} \equiv \int_0^1 a(s)\,ds = \frac{\exp(\alpha\psi)^2}{\sqrt{2}\alpha}\left\{\frac{\cosh(\sqrt{2}\,\alpha\gamma)\sinh(\sqrt{2}\,\alpha\gamma)}{\exp[\tanh^2(\sqrt{2}\alpha\gamma)/2]} + \frac{\sqrt{\pi}}{2}\left[\operatorname{erf}(\alpha\psi) - \operatorname{erf}\left(\frac{\tan(\sqrt{2}\alpha\gamma)}{\sqrt{2}}\right)\right]\right\} \tag{35}$$

Equation (35) is plotted versus α in Fig. 5 and compared, in the higher range, with the corresponding fully stressed designs. Although the separation between the two is not significant until α exceeds approximately 1.5, nevertheless the rapidly rising weight of both leads one to suspect that better designs might be discovered than these, requiring as they do large amounts of material to force ω_1 to exceed ω_e.

Note, from Fig. 4, that over their entire length the dynamic solutions display areas larger than what would withstand the same force applied statically ($\alpha = 0$). This explains why no minimum-area constraint seemed necessary for the first-mode analysis.

Second-Mode Solutions ($\alpha > \alpha_1$)

As discussed further in Sec. V, the response of the bar in the frequency range $\omega_1 < \omega_e < \omega_2$ must be in antiphase with the applied load, i.e., $x_1(s) \leq 0$, except possibly in a small region near the tip. It can then be reasoned that a tip mass may be required ($a_T \neq 0$) to satisfy boundary condition (12). It

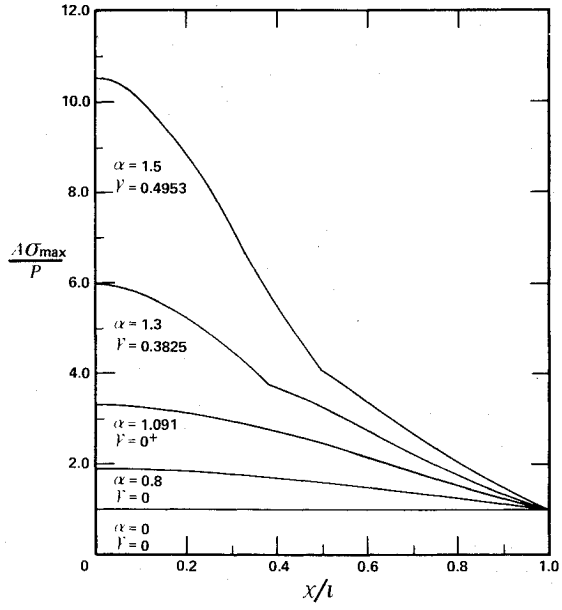

Fig. 4 Dimensionless cross-sectional area distributions of the first-mode optimal designs, plotted vs distance along the bar for five values of frequency parameter α.

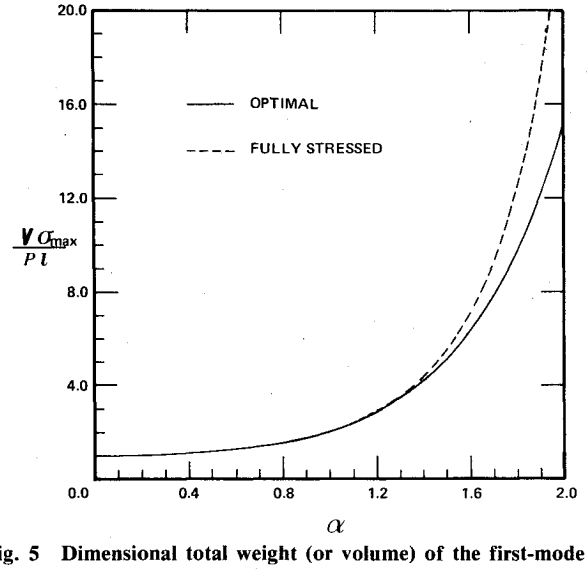

Fig. 5 Dimensional total weight (or volume) of the first-mode optimal designs as a function of α. Above $\alpha = 1.0908$, the fully stressed design is shown for comparison.

definitely proves necessary to enforce the minimum-gauge constraint (14) to avoid a tendency toward vanishing area at the point of zero slope in the response mode $x_1(s)$.

Without reproducing all mathematical details (see Ch. 4, Ref. 11), one determines that the optimal solution consists of two arcs: stress constraint active in $0 \le s \le \gamma$ and minimum-area constraint active in $\gamma \le s \le 1$. Its characteristics are worked out (as above) by first solving in the two ranges separately, then fixing several unknown constants by trial-and-error matching of transcendental relations at $s = \gamma$. Since a_T is retained in Eq. (12), its optimal determination becomes an organic part of the process.

Figure 6 displays the resulting values of γ, plotted versus α for a wide selection of minimum-gauge parameters $\delta = P/A_{min}\sigma_{max}$. For too large α values, at any given δ, the Lagrange multiplier μ_2 is no longer positive throughout the entire tip arc. This limitation is expressed by the broken line in Fig. 6. Its onset indicates that more than two arcs are needed in the optimal design – a situation discussed subsequently.

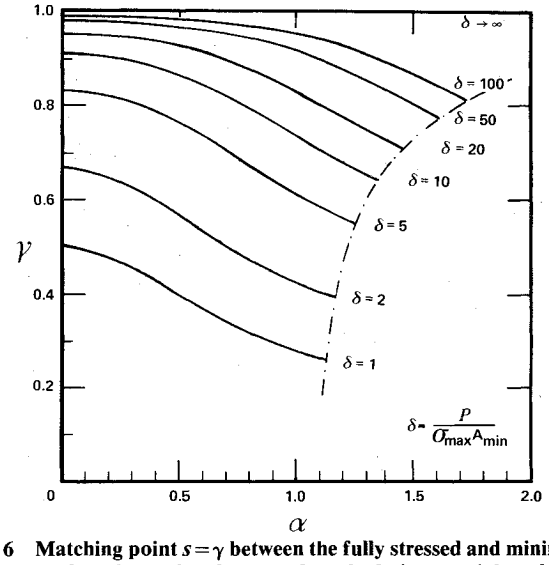

Fig. 6 Matching point $s = \gamma$ between the fully stressed and minimum-area arcs, plotted vs α for the second-mode designs at eight values of parameter δ.

With γ specified, the dimensionless area distribution is

$$a = \begin{cases} \dfrac{\exp[\alpha^2(\gamma^2 - s^2)]}{\delta}, & 0 \le s \le \gamma \\ 1/\delta, & \gamma \le s \le 1 \end{cases} \tag{36}$$

whereas the tip-mass parameter is

$$a_T = \frac{1}{\sqrt{2}\,\delta\alpha}\left\{\frac{\delta + \cos[\sqrt{2}\alpha(1-\gamma)] - \sqrt{2}\gamma\alpha\,\sin[\sqrt{2}\alpha(1-\gamma)]}{\sin[\sqrt{2}\alpha(1-\gamma)] + \sqrt{2}\gamma\alpha\,\cos[\sqrt{2}\alpha(1-\gamma)]}\right\} \tag{37}$$

From Eqs. (36) and (37), one may compute the total weight parameter

$$\frac{V\sigma_{max}}{P\ell} \equiv a_T + \int_0^1 a(s)\,ds = \frac{1}{\delta}\left(\frac{\sqrt{\pi}}{2\alpha}e^{(\alpha\gamma)^2}\mathrm{erf}(\alpha\gamma) + 1 + \frac{\delta + (1 - 2\alpha^2\gamma^2)\cos[\sqrt{2}\alpha(1-\gamma)] - 2\sqrt{2}\alpha\gamma\,\sin[\sqrt{2}\alpha(1-\gamma)]}{\sqrt{2}\alpha\{\sin[\sqrt{2}\alpha(1-\gamma)] + \sqrt{2}\alpha\gamma\,\cos[\sqrt{2}\alpha(1-\gamma)]\}}\right) \tag{38}$$

Figure 7 plots the optimal $a(s)$ (and a_T on the right-hand scale) for two δ values and $\alpha = 1.0$, 1.3. Perhaps more interesting are the Fig. 8 data on dimensionless total weight, Eq. (38). Here the first-mode curve from Fig. 5 is also reproduced. When $\alpha < 0.63$, the latter proves superior to any possible second-mode solution. At higher forcing frequencies, on the other hand, a selection of designs with $\omega_1 < \omega_e$ is available that can save substantial weight.

A surprising mathematical feature of the second-mode solutions is the discontinuous behavior of Lagrange multipliers μ_1 and μ_2 at the matching point $s = \gamma$. An error was first suspected with the discovery that μ_1 drops from a finite positive value to zero when passing outboard across $s = \gamma$, whereas μ_2 jumps from zero to just the size needed to make H and $\partial H/\partial a$, Eqs. (17) and (18), properly continuous. It was subsequently observed that the last two terms in Eq. (17) might as well have been written

$$\mu_1\left[\frac{|x_2|}{\beta} - a\right] + \mu_2\left[\frac{1}{\delta} - a\right]$$

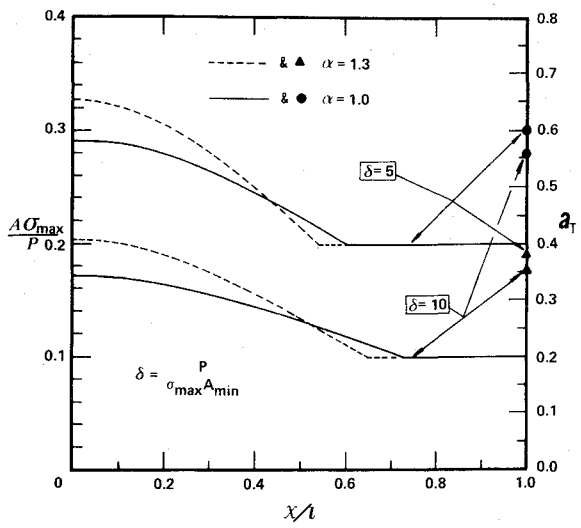

Fig. 7 Dimensionless cross-sectional area distributions of the second-mode optimal designs, plotted vs distance along the bar for two values each of α and δ. The corresponding dimensionless tip masses a_T are indicated on the right-hand ordinate.

and might have been interpreted as a single adjoined constraint of the general form

$$\mu[f(x_2)-a]$$

The discontinuity in μ itself is then found to disappear. At $s=\gamma$, there are slope discontinuities in $\mu(s)$, $a(s)$, and the function f, but such phenomena are acceptable and often encountered in control-theory applications.

V. Normal Modes of the Optimal Designs: Relationship Between Forced and Free-Mode Shapes

Further examination of the free and forced motions of the continuous bar is useful, both to interpret the foregoing results and to assist with speculation as to how they might be extended. From Eqs. (4) and (5), one sees that the ith normal mode and frequency must satisfy

$$\frac{d}{ds}\left[a(s)\frac{du_i}{ds}\right]+2\alpha_i^2 u_i=0 \tag{39}$$

subject to the boundary conditions

$$u_i(0)=0 \tag{40a}$$

$$a(1)\frac{du_i(1)}{ds}=2\alpha_i^2 a_T u_i(1) \tag{40b}$$

If a variable change $t=\alpha s$ is performed and the fully stressed area distribution ($\alpha \le 1.0908$)

$$a(s)=\exp[\alpha^2(1-s^2)]\rightarrow a(t)=\exp(\alpha^2-t^2) \tag{41}$$

is inserted into Eqs. (39) and (40) one is led to the equation and transformed boundary conditions

$$\frac{du_i^2}{dt^2}-2t\frac{du_i}{dt}+2\eta_i u_i=0 \tag{42}$$

$$u_i(0)=0 \tag{43a}$$

$$\frac{du_i(\alpha)}{dt}=2\eta_i\alpha\frac{a_T}{a(\alpha)}u_i(\alpha) \tag{43b}$$

where

$$\eta_i=(\alpha_i/\alpha)^2 \tag{44}$$

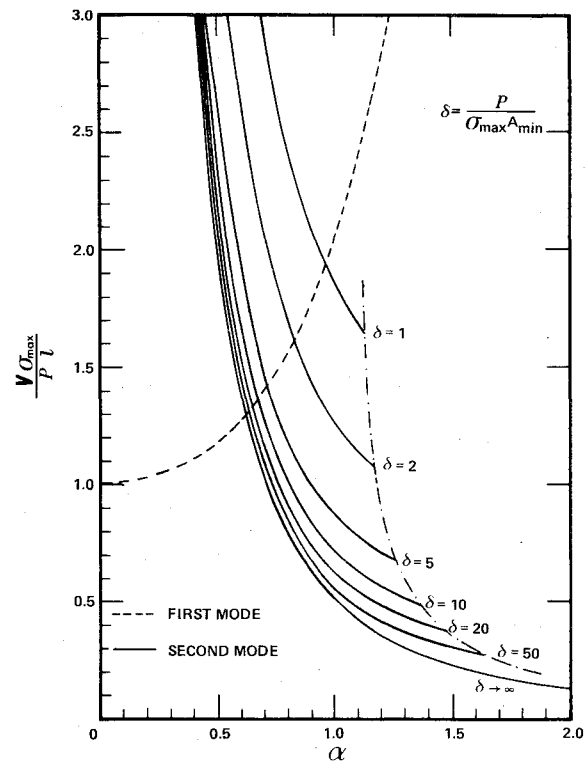

Fig. 8 Dimensionless total weight (or volume) of the second-mode optimal designs as a function of α and δ. The first-mode curve from Fig. 5 is shown dotted. To the right of the dash-dot line, the two-arc solutions of Sec. IV are no longer optimal.

Equation 42 is solved by nonintegral Hermite functions (see, e.g., Ref. 16, p. 322). As worked out in Ref. 11 (Chapt. 4), condition (43a) eliminates one of the two independent solutions, whereas Eq. (43b) (for $a_T=0$) yields the characteristic relation

$$0=1+\sum_{n=1}^{\infty}2^n\frac{[\alpha^2-\alpha_1^2][3\alpha^2-\alpha_1^2]\ldots[(2n-1)\alpha^2-\alpha_1^2]}{(2n)!} \tag{45}$$

Only if $\alpha_1>\alpha$ can Eq. (45) be satisfied, since otherwise every term in the summation would be positive.

In Fig. 9, α_1, α_2, and α_3 are given as functions of α for the first-mode optimal bars. These numbers were estimated from Eq. (45) for $\alpha \le 1.0908$ and computed numerically from Eqs. (39) and (40) at higher forcing frequencies. One observes the anticipated behavior, ever-heavier bars being forced increasingly closer to resonance with the fundamental mode as α becomes unnaturally large for these first-mode designs.

In Ref. 11 (Chapt. 4), a similar calculation is carried out for the second-mode bars. Some results for the first two natural frequencies appear in Fig. 10, with the minimum-gauge parameter chosen as $\delta=10$. In this example, it is seen, as expected, that the forcing frequency always falls between the fundamental ω_1 and the first harmonic ω_2. As in Fig. 9, there is a tendency with increasing α for the "optimal" natural frequencies to be driven away from the resonance line. But here the undesirable asymptotic convergence of α to α_2 would not set in until the former approached twice the magnitude covered by the Fig. 10 calculations.

Curiosity impels one to investigate not only the behavior of the second-mode solutions to the right of the limit in Fig. 8 but also what might happen in ranges $\alpha_i<\alpha<\alpha_{i+1}$, where $i>1$. Considerable light can be thrown on such questions by means of a modest extension of the Sturm-Liouville analysis, which determines the relationships between the forced mode shapes $u(x)$ and their adjacent normal modes $u_i(x)$. An excellent summary of the normal mode analysis is given by Morse and Feshbach.[17]

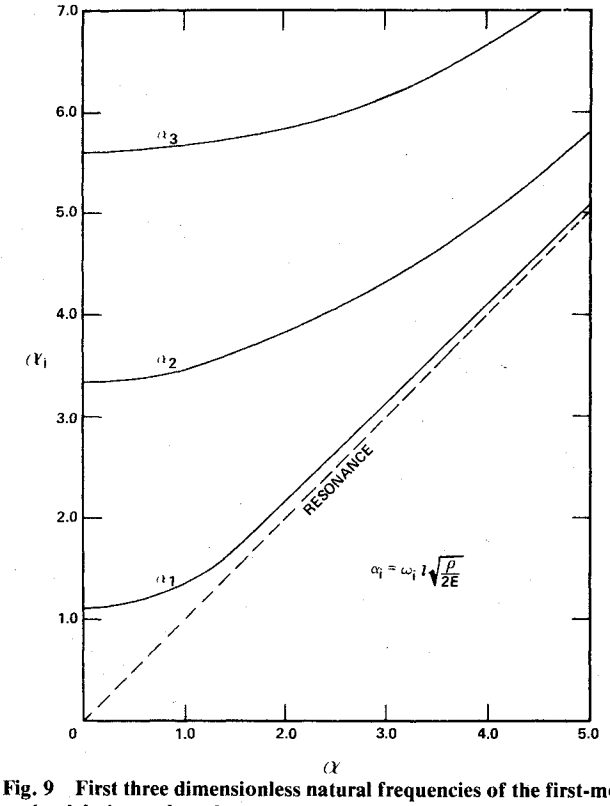

Fig. 9 First three dimensionless natural frequencies of the first-mode optimal designs, plotted vs α.

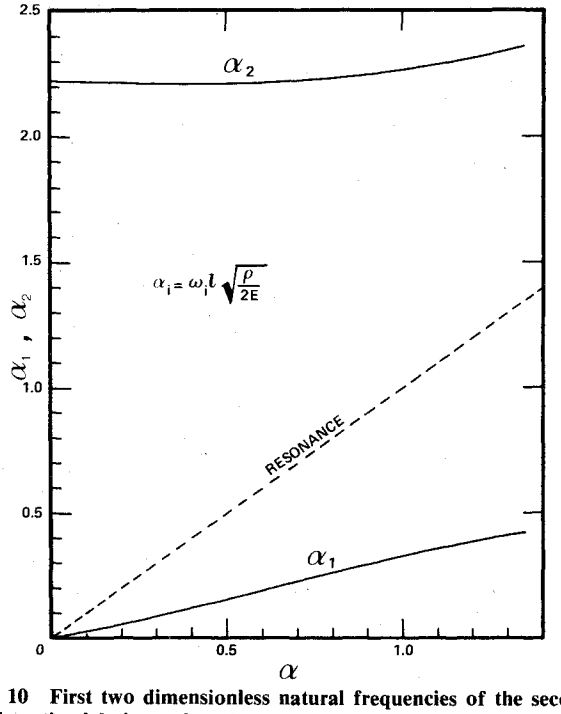

Fig. 10 First two dimensionless natural frequencies of the second-mode optimal designs, plotted vs α.

Using their approach, Rizzi[11] (Chapt. 4) proves that the zeros (if any) of $u(x)$ are bracketed by the nodes $u_i = 0$ of those normal modes whose frequencies bracket the forcing frequency ω_e. This finding is illustrated in Fig. 11 for the first- and second-mode optimal designs. Since $u_1(x)$ has no nodes and zero slope at its unloaded tip, the first-mode response must also be entirely above the x axis. Its positive tip slope is necessary to counterbalance the effect of the applied oscillatory force.

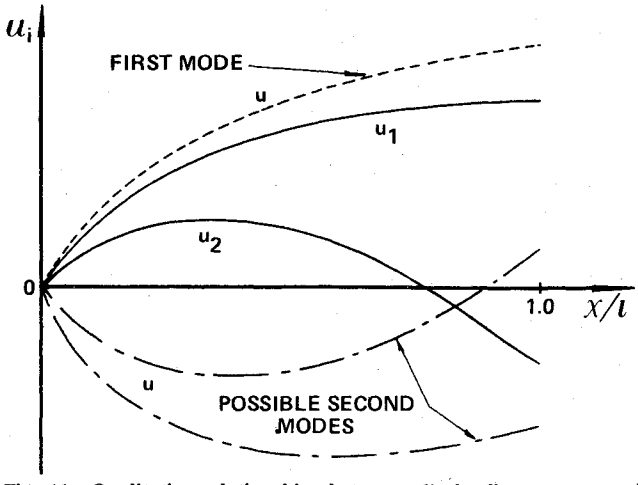

Fig. 11 Qualitative relationships between: 1) the first two normal mode shapes of a cantilever bar, and 2) possible first- and second-mode forced response amplitudes $u(x)$ due to tip excitation.

As for the second-mode solution, whose frequency falls in $\omega_1 < \omega_e < \omega_2$, it may have zero or one node, but the latter must fall closer to the tip than the single node that $u_2(x)$ has to have.[17] This relationship is shown in Fig. 11, as is another fact proved by Rizzi: the second response mode $u(x)$ must start from $x=0$ with negative slope and therefore remain below the x axis until outboard of the node location. If this mode has zero nodes, its tip slope may be positive (as in Fig. 11) or negative. Incidentally, this last observation explains the need for a tip mass as part of all the second-mode solutions worked out quantitatively here.

VI. Higher Mode Solutions

The foregoing offers a key to the difficulties that may be encountered when seeking optimal designs for the continuous bar at higher frequencies. Since each normal mode shape $u_{i+1}(x)$ is known to have one more node than its predecessor, the forced-response mode shapes will also be progressively more sinuous. Thus, for $\omega_2 < \omega_e < \omega_3$, there will be one or two nodal points; for $\omega_3 < \omega_e < \omega_4$, there will be two or three, etc. This has the effect that the optimal solutions will be composed of increasing numbers of differently constrained arcs, with increasingly complicated algebraic manipulations demanded by the matching of their various properties at the points of junction. To illustrate, for $\alpha > 1.0908$, the first-mode solution of Sec. IV consists of a fully stressed arc outboard of an unconstrained arc. Its corresponding $u(x)$ consists of a rectilinear segment outboard of a hyperbolic-sine segment, so that du/dx grows monotonically from root to tip; obviously no node would be possible. The second-mode solution is a minimum-area arc outboard of a fully stressed one, i.e., a sine curve matched to the end of a straight line.

Both confirmation of the foregoing results for the continuous bar and evidence of the behavior for higher values of α have been obtained by the use of finite element approximations. Rizzi[11] coupled a finite element model of the axially forced bar with an efficient optimality criterion algorithm to determine finite element approximations to the optimal thickness distributions. (See Ref. 11 for several calculations that confirm Fig. 3-8.) Figure 12 plots a second mode a distribution computed with 20 constant property elements of equal length (see Fig. 1b). The parameters used in Fig. 12, $\alpha = 2.0$ and $\delta = 10$ ($a_{\min} = 0.1$), fall well out of the range where the two arc continuum solutions of Sec. IV are optimal (see Fig. 6). The dimensionless weight of 0.342 does, however, appear to lie roughly on an extrapolation of the curve in Fig. 6. There is an outboard mass concentration in this design, but the indication is that an actual tip mass is no longer required for optimality at this high α value. Plotted in Fig. 13 is the response mode $u(x)$ corresponding to the area

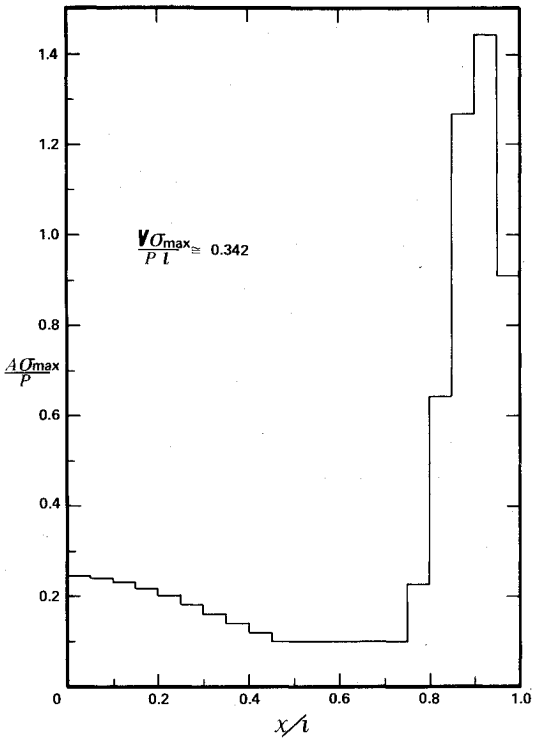

Fig. 12 Finite-element optimal solution for $n=20$, $\alpha=2.0$, and $\delta=10$.

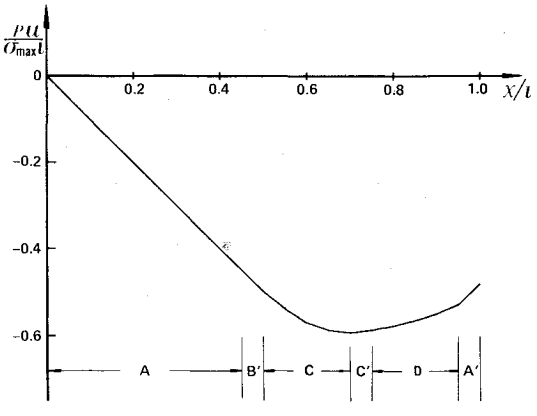

Fig. 13 Mode shape of forced response for the Fig. 13 design (meaning of segments, A, B′, etc., discussed in text).

distributions of Fig. 12. As well as can be determined from this discretized solution, this is a case of three matched arcs. Over the segment marked A, $u(x)$ is a perfectly straight line with the stress constraint active. The elements between $(x/\ell)=0.45$ and 0.75 are at a_{min} so that in the arc approximately defined by C, the minimum-gauge constraint applies and $u(x)$ has the expected sinusoidal shape with a maximum deflection at $x/\ell=0.75$. Neither constraint is active on arc D, but the length is too short to ascertain whether $u(x)$ is behaving like the hyperbolic functions encountered in the unconstrained arcs of the first mode solutions of Sec. IV. Finally, the single elements B', C', and A' are arbitrarily designated as matching zones plus a zone for adjustment to the tip boundary condition. They would be expected to shrink to points for an infinite number of finite elements.

It is clear that if the continuous bar corresponding to Figs. 12 and 13 were sought, three arcs would have to be specified. The matching point locations γ_1 and γ_2 would be among the 10 or more unknowns to be found from a set of transcendental matching relations. The authors are not yet in a position to say whether an analytical solution to this nonlinear system exists. In any event, a very tedious calculation would be called for, and one reluctantly concludes that some numerical technique, whether it be finite element or a numerical integration scheme, is the "path of least resistance." With regard to numerical integration, a recent paper by Ohlhoff[18] develops methods for the optimization of beams with respect to higher order natural frequencies that are almost directly applicable to this problem. Ohlhoff treats the matching points as additional control parameters in the determination of the optimal area distributions.

Finally, the behavior of the higher mode solutions over the entire range of excitation frequencies, $0\leq\alpha\leq\infty$, can be studied by the use of another two-design-variable example shown to the authors by Prof. A. E. Bryson. In this example, the dimensionless variables used are a *constant* area rod, a, with an attached tip, mass, a_T. The problem statement of Sec. II remains unchanged except that the cost function of Eq. (1) is now simply $a+a_T$. As proved by Rizzi,[11] the optimal solution with this formulation is the minimum of two possible designs

$$1)\quad a=|\sec\sqrt{2}\alpha|\ ,\qquad a_T=0 \tag{46}$$

$$2)\quad a=1/\delta,\qquad a_T=\frac{1+1/\delta\,\cos\sqrt{2}\alpha\,\operatorname{sgn}(\sin\sqrt{2}\alpha)}{\sqrt{2}\alpha\,|\sin\sqrt{2}\alpha|} \tag{47}$$

The volumes of these two alternatives are plotted in Fig. 14, along with the corresponding variable area results from Sec. IV. It is seen that the two-design-variable case furnishes a good approximation to the more complicated variable-area result; in fact, it provides a useful upper bound in the search for variable area optima.

For the two-design-variable case, the Eq. (46) solution, which is designated "type one" and has no tip mass, is seen to be optimal for the lowest values of α. This corresponds to the "first mode" results of Sec. IV. At $\alpha\cong0.75$, the second type of solution, i.e., a minimum area rod with a non-zero tip mass, becomes optimal, corresponding to the "second mode" results of Sec. IV. At $\alpha\cong2.0$, the first type again takes over. It roughly corresponds to the finite-element solution of Figs. 12 and 13, where apparently no tip mass is required. Above $\alpha\cong2.5$, the second design is optimal, with the excitation frequency greater than the first two natural frequencies, $\alpha_2<\alpha<\alpha_3$. In the terminology of Sec. IV, this is a "third mode" solution.

If the designs of Eqs. (46) and (47) were plotted for even higher values of α, it would be seen that this switching from one type of solution to another continues, resulting in a scalloped pattern for the optimal volume as a function of excitation frequency. The authors would like to suggest that a similar pattern would appear for the variable area rod if the curve of Fig. 8 could be extended to higher α's.

VII. Discussion and Conclusions

Although this paper deals primarily with exploration of the current limits of function-space optimization as related to one-dimensional elastic continua, the question of practical applications needs to be addressed. In seeking them, one turns to structures intended for dynamic force transmission, vibration, isolation, and shock mounting. In many earth-bound devices, the motivation toward saving weight hardly exists, and designers may be expected to stick, as in the past, with uniform rods, beams, bars, etc. Not so for aeronautical and space vehicles, where every newton of weight may count. There are other surface and marine transportation systems where weight minimization may be required; submarine propeller shafts are an obvious possibility.

To be rigorous, the present designs seem limited to the following circumstances:

a) The applied tip force or torque is transmitted from its source through an essentially massless medium, like a soft spring.

b) Sinusoidal loads predominate over any starting or stopping transients.

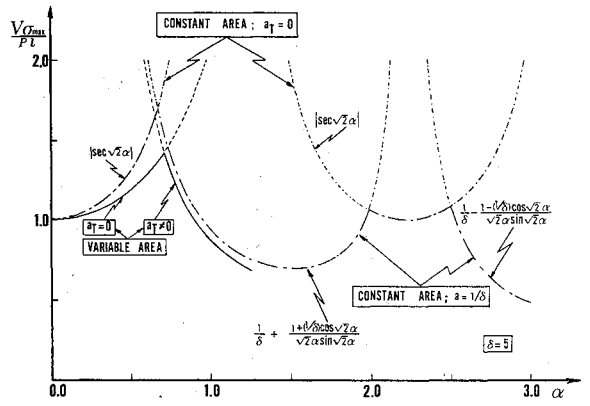

Fig. 14 Comparison of optimal dimensionless weights (or volumes) obtained with variable and constant cross-sectional area, $\delta = 5$.

c) The internal stresses due to any static loadings are outweighed by the dynamic stresses.

These conditions do not occur together in many practical situations. On the other hand, b and c often apply to a shear-beam or torsional vibration isolator, which supports an engine or machine tool containing some reciprocating source of excitation. In "soft mounting," some very large vibratory stresses may be superimposed on the essentially static stress due to the weight and/or they may be in another direction. Then it appears that the present designs might be used, with only the addition of a prescribed tip mass M_T. So far as the mathematics is concerned, such a modification is almost trivial.

This suggested extension is one of several that come to mind, wherein continuous structures are involved and the methods borrowed from optimal control theory retain their potency. Other boundary conditions such as simple support may be invoked. Distributed external loads are encountered nearly as often as concentrated ones. There are tractable examples, such as thick-walled or solid rods, where the design variable does not enter certain equations linearly, as $a(s)$ does here. Finally, the fourth-order differential equations that govern beamlike structures may also be successfully tackled, albeit numerical integration then becomes inevitable.

Some direct conclusions from what has already been done are as follows:

a) Variational calculus techniques, as adapted from the automatic control literature, provide a valuable tool to design one-dimensional structures under certain classes of dynamic loading. Although not as effective as, e.g., energy methods in providing sufficient conditions for global optimality, they enable one to penetrate barriers like that which hitherto limited $\omega_e < \omega_1$.

b) The natural frequencies of the structure play a central role in creating many local optima and, in the absence of damping, multiple feasible regions. Since there are no *a priori* ways to identify the global best design, solution methods must be capable of finding and computing more than one.

c) It is often necessary to specify minimum-gauge constraints to ensure meaningful optima.

d) A concentrated mass must sometimes be included in a design to satisfy a boundary condition, although it is not felt that they will be required at interior parts.

e) When more than two different constrained arcs characterize the optimal solution, the continuum approach may be impractical. This remains a challenge for the future. Finite-element approximations then offer the only alternative. Special care must be taken both in modeling and in the optimal search; frequency-range constraints will be needed to isolate various local optima associated with higher forcing frequency.

References

[1]Bryson, A. E. and Ho, Y. C., *Applied Optimal Control*, Hemisphere Publishing Corp., Washington, D.C., 1975.

[2]Sheu, C. Y. and Prager, W., "Recent Developments in Optimal Structural Design," *Applied Mechanics Review*, Vol. 21, No. 10, Oct. 1968, pp. 985-992.

[3]Gellatly, R. A., Ed., *Structural Optimization*, AGARD Lecture Series 70, Hampton, Va., Oct. 1974.

[4]Schmit, L. A., Jr., Ed., *Structural Optimization Symposium*, American Society of Mechanical Engineers, New York, Nov. 1974.

[5]Pierson, B. L., "A Survey of Optimal Structural Design Under Dynamic Constraints," *International Journal for Numerical Methods in Engineering*, Vol. 4, July-Aug. 1972, pp. 491-499.

[6]Rao, S. S., "Optimum Design of Structures Under Shock and Vibration Environment," *The Shock and Vibration Digest*, Vol. 7, Dec. 1975, pp. 61-70.

[7]Icerman, L. J., "Optimal Structural Design for Given Dynamic Deflection," *International Journal of Solids and Structures*, Vol. 5, May 1969, pp. 473-490.

[8]Mroz, Z., "Optimal Design of Elastic Structures Subjected to Dynamic, Harmonically Varying Loads," *Zeitschrift fur Angewandte Mathematik und Mechanik*, Vol. 50, May 1970, pp. 303-309.

[9]Plaut, R. H., "Optimal Structural Design for Given Deflection Under Periodic Loading," *Quarterly of Applied Mathematics*, Vol. 29, July 1971, pp. 315-318.

[10]Johnson, E. H., "Optimization of Structures Undergoing Harmonic or Stochastic Excitation," PhD Dissertation, Dept. of Aeronautics and Astronautics, Stanford University, Stanford, Calif., June 1975.

[11]Rizzi, P., "The Optimization of Structures with Complex Constraints Via a General Optimality Criteria Method," PhD Thesis, Dept. of Aeronautics and Astronautics, Stanford University, Stanford, Calif., July 1976. (The dissertations mentioned in Refs. 10 and 11 were recently published, along with a third by Dr. S. Segenreich, as SUDAAR 501, Stanford University Dept. of Aeronautics and Astronautics, Stanford, Calif., 94305, Aug. 1976.)

[12]Timoshenko, S. and Young, D. H., *Elements of Strength of Materials*, Van Nostrand Co., New York, 1962, p. 225.

[13]Cassis, J. H., "Optimum Design of Structures Subjected to Dynamic Loads," UCLA-ENG-7451, UCLA, School of Engineering and Applied Science, June 1974.

[14]Segenreich, S. A. and Rizzi, P., "Properties of Axial or Torsional Free-Vibrational Frequencies of Rods," *AIAA Journal*, Vol. 13, Aug. 1975, pp. 1111-1112.

[15]Johnson, E. H., "Disjoint Design Spaces in the Optimization of Harmonically Excited Structures," *AIAA Journal*, Vol. 14, Feb. 1976, pp. 259-262.

[16]Murphy, G. M., *Ordinary Differential Equations and Their Solutions*, Van Nostrand Reinhold Co., New York, 1960.

[17]Morse, P. M. and Feshbach, H., *Methods of Theoretical Physics*, McGraw-Hill, New York, 1953, pp. 719-724.

[18]Ohlhoff, N., "Optimization of Vibrating Beams with Respect to Higher Order Natural Frequencies," *Journal of Structural Mechanics*, Vol. 4, Jan. 1976, pp. 87-122.